Inorganica Chimica Acta 380 (2012) 252–260

Contents lists available at SciVerse ScienceDirect

Inorganica Chimica Acta

journal homepage: www.elsevier.com/locate/ica

Synthesis and coordination chemistry of pyrimidine-substituted phosphine ligands

Tracy D. Nixon, Aimee J. Gamble, Robert J. Thatcher, Adrian C. Whitwood, Jason M. Lynam *

Department of Chemistry, University of York, Heslington, York YO10 5DD, UK

ARTICLE INFO

Article history:
Available online 29 October 2011

Young Investigator Award Special Issue

Keywords:
Phosphine ligands
Hydrogen bonding
Ruthenium half sandwich

ABSTRACT

Reaction of PPh_2H with UrI (Ur = uracil) in the presence of $Pd(OAc)_2$ affords PPh_2Ur. In the solid state, PPh_2Ur crystallises as a methanol solvate in the monoclinic space group $P2_1/c$. Reaction of PPh_2Ur with CuI in dry and deoxygenated THF solution results in the formation of $[Cu_4(\mu_3\text{-}I)_4(PPh_2Ur)_4]$. A single crystal X-ray diffraction study demonstrated that this species contains a distorted tetrahedral core of copper atoms, with facially-capping iodides. The uracil groups in the clusters are engaged in hydrogen bonding to groups on neighbouring molecules to form an extended array. A similar reaction between PPh_2Ur and CuI in unpurified THF allows for the isolation of the phosphine oxide $P(O)PPh_2Ur$. The synthesis of the benzyl-protected phosphine PPh_2Ur^P is also described [Ur^P = 2,4-bis(benzyloxy)pyrimidine]. Reaction of PPh_2Ur^P with $[Ru(\eta^5\text{-}C_5H_5)(NCMe)_3]PF_6$ allows for isolation of $[Ru(\eta^5\text{-}C_5H_5)(NCMe)(PPh_2Ur^P)_2]PF_6$.

1. Introduction

Phosphorus(III) ligands play a pivotal role as co-ligands in transition metal chemistry [1]. Variation of the substituents in the PR_3 framework allows for direct control over the steric and electronic effects exerted by the ligand and, therefore, the properties of any resulting metal complex. Indeed metrics such as cone angle and the Tolman electronic parameter have ensured that phosphorus(III) ligands may be used to develop well-defined structure–activity relationships [2]. Furthermore, a number of additional approaches to determining the steric and electronic influence of these ligands have been developed [3].

The introduction of additional functional groups into the ligand framework may be employed to generate more diverse control over the reactivity of transition metal compounds. For example, the introduction of *N*-heterocycles into the P(III) ligand may be used to position a Brønsted basic site in close proximity to the metal [4]. This basic position has subsequently been shown to facilitate proton transfer reactions in organic ligands bound to the metal. Furthermore, phosphorus-based ligands that may engage in mutually complementary hydrogen-bonding in the coordination sphere of the metal have been shown to increase both the selectivity in rhodium-catalysed hydroformylation [5] and the anti-Markovnikov hydration of terminal alkynes [6].

We have previously demonstrated that the incorporation of pendant uracil groups into the coordination sphere of metal compounds may be used to dictate the assembly of both organometallic and coordination compounds in the solid state and solution [7]. For example, reaction of ruthenium half sandwich compounds with HC≡CUr may be employed to prepare the vinylidene-containing complex $[Ru(\eta^5\text{-}C_5H_5)(=C=CHUr)(PPh_3)_2][PF_6]$ which, in the solid state, self-assembles to give a remarkable hexameric motif [8]. The presence of the uracil substituent does not profoundly alter the underlying organometallic chemistry of the half-sandwich compound. For example complexes containing carbene, alkynyl and alkenyl ligands, all containing pendant uracil groups, may be prepared in a similar vein to their phenyl-substituted analogues [9]. In addition, this method may be applied to the preparation of square-planar and half-sandwich rhodium compounds, again with the uracil dictating assembly in both the solid state and solution [10].

Given that suitable phosphine ligands may employ non-covalent interactions to dictate the behaviour of transition metal compounds, we sought to expand this methodology to phosphorus-based ligands containing pendant uracil groups. The methodology which we had developed using HC≡CUr as a substrate had demonstrated that an appropriate choice of metal would ensure that selective binding to the alkyne occurred, it was envisaged that a similar strategy might translate to phosphorus-based ligands. The synthesis of the uracil-substituted phosphine PPh_2Ur was therefore targeted. It is important to note that Kamer and co-workers have demonstrated that it is possible to incorporate PPh_2 groups into the backbone of deoxyuridine units that are part of an oligonucleotide [11]. This phosphine ligand is able to introduce a measure of enantiocontrol in palladium-mediated allylic-substitution reactions.

The synthesis of the uracil-substituted phosphine PPh_2Ur is now reported with the resulting copper(I)iodide complex, along with the corresponding oxide, $P(O)Ph_2Ur$. Furthermore the preparation of a phosphine ligand containing a protected uracil group,

* Corresponding author. Tel.: +44 (0) 1904 322534; fax: +44 (0) 1904 322516.
E-mail address: jason.lynam@york.ac.uk (J.M. Lynam).

0020-1693/$ - see front matter © 2011 Elsevier B.V. All rights reserved.
doi:10.1016/j.ica.2011.10.058

PPh_2Ur^P, and the ruthenium complex $[Ru(\eta^5\text{-}C_5H_5)(NCMe)(P\text{-}Ph_2Ur^P)_2][PF_6]$ are also described. In a preliminary communication we have shown that the gold phosphine complex $AuCl(PPh_2Ur)$ self-assembles in the solid state to give a crystalline structure with large solvent-accessible areas [12]. This solid state structure is dictated by hydrogen bonding interactions between uracil groups on neighbouring molecules. The resulting array is robust and it appeared to be possible to remove and replace the solvent from these areas without substantial degradation in the quality of the crystalline material.

2. Results and discussion

2.1. Synthesis of PPh_2Ur

The uracil-substituted phosphine PPh_2Ur may conveniently be prepared by the palladium-catalysed coupling of PPh_2H with 5-iodouracil in DMF solution at 60 °C in the presence of triethylamine (Scheme 1). The compound was obtained as colourless crystals that proved to be soluble in DMSO, THF, warm MeOH and acetone, partially soluble in $CHCl_3$ and insoluble in water, hexane, toluene and diethylether. Crystals of PPh_2Ur suitable for study by X-ray crystallography were obtained from a methanol solution of the phosphine. The resulting structure determination revealed that PPh_2Ur had crystallised as a methanol solvate and the asymmetric unit is shown in Fig. 1. An examination of the structure revealed that the PPh_2Ur unit possessed the expected connectivity, with the PPh_2 group being attached to the 5-position of the uracil. The introduction of the uracil group only introduces small distortions in the structure of the phosphine ligand. For example, the bond angles surrounding phosphorus are similar [(C(4)–P(1)–C(11) 103.09(7)°, C(4)–P(1)–C(5) 101.03(7)°, C(11)–P(1)–C(5) 101.04(7)°], although the sum of the angles at phosphorus [305.19(12)°] is somewhat less than that seen in PPh_3 [308.21(13)° [13] 308.57(10)° [14] and 308.18(14)° [15]]. There is some asymmetry in the P–C bonds with that between the phosphorus and the uracil group [C(4)–P(1) 1.8208(15) Å] being notably shorter than those to the phenyl groups [C(5)–P(1) 1.8365(15) Å, C(11)–P(1) 1.8291(16) Å].

As shown in Fig. 2a, the uracil groups of the phosphine ligands engage in complementary hydrogen-bonding between the N–H group in the 1-position of the uracil and the carbonyl group in the 2-position [N(2)–H(19)···O(2) 2.771(2) Å; H(19)···O(2) 1.89(2) Å]. In addition the remaining N–H and carbonyl groups in the uracil are involved in hydrogen bonding with the oxygen and hydrogen of the OH group of the methanol respectively [N(1)–H(18)···O(3) 2.742(2) Å, H(18)···O(3) 1.86(3) Å, O(3)–H(3A)···O(1) 2.763(2) Å, H(3A)···O(1) 1.96(3) Å]. The combination of these interactions results in the formation of stacks of dimeric PPh_2Ur units linked by methanol molecules. Neighbouring stacks run in orthogonal directions. A space-filing model of the structure of PPh_2Ur (Fig. 2b) viewed down the *c*-axis of the unit cell illustrates the polar domains (containing the uracil and methanol groups) and non-polar areas (the phenyl groups of the phosphine).

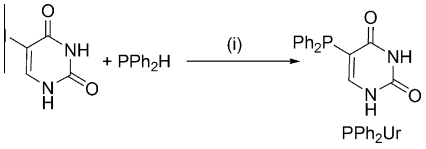

Scheme 1. (i) $+Pd(OAc)_2$, $+NEt_3$, $-[NHEt_3]I$, DMF, 60 °C 1 h.

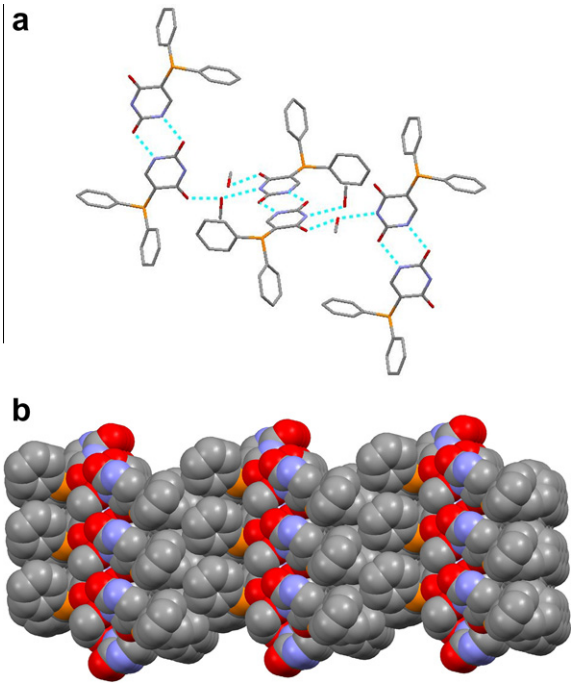

Fig. 2. (a) Hydrogen bonding interactions in the structure of $PPh_2Ur{\cdot}MeOH$. (b) Space filling diagram of $PPh_2Ur{\cdot}MeOH$.

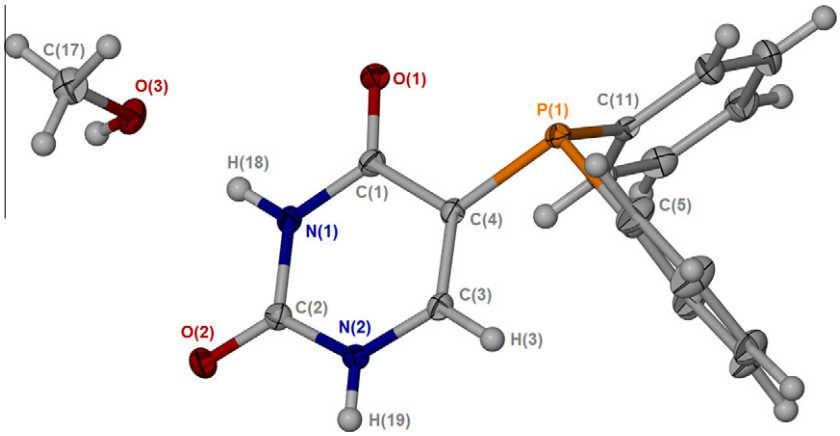

Fig. 1. Molecular structure of PPh_2Ur as the methanol solvate as determined by single crystal X-ray diffraction. Thermal ellipsoids are shown at the 50% probability level.

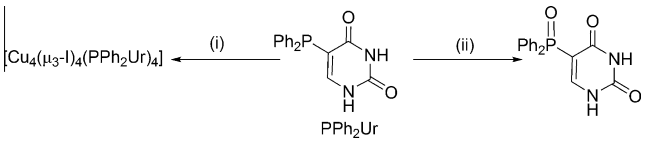

Scheme 2. (i) +CuI, purified THF; (ii) +CuI, reagent-grade THF.

2.2. Reaction of PPh_2Ur with CuI

The reaction of CuI with PPh_2Ur in THF solution resulted in the formation of a tetrameric complex $[Cu_4(\mu_3\text{-}I)_4(PPh_2Ur)_4]$. In order for the reaction to be successful it was imperative to employ purified THF as the use of reagent grade solvent only allowed for the phosphine oxide $P(O)PPh_2Ur$ to be isolated, Scheme 2 (see Section 2.3).

The copper complex was isolated as colourless crystals suitable for study by X-ray diffraction. The resulting structural determination demonstrated that $[Cu_4(\mu_3\text{-}I)_4(PPh_2Ur)_4]$ had co-crystallised as a THF solvate. Unfortunately, due to problems with disorder only two of the THF molecules in the asymmetric unit could be successfully modelled. The structure of the copper core of this system is shown in Fig. 3a, and the hydrogen bonded network in Fig. 3b.

The $[Cu(\mu_3\text{-}I)P]_4$ core of the complex may be considered to be a distorted tetrahedron of copper atoms each bound to a terminal phosphine ligand with facially capping iodide ligands: selected bond lengths are presented in Table 1. There are considerable deviations from an ideal tetrahedron with Cu···Cu distances ranging from 3.0361(6) Å [Cu(1)···Cu(3)] to 2.8235(6) Å [Cu(2)···Cu(4)]. The distorted tetrahedral copper core is similar to that reported by Churchill and Rotella [16] for $[Cu_4(\mu_3\text{-}I)_4(PPh_2Me)_4]$ but differs from $[Cu_4(\mu_3\text{-}I)_4(PPh_3)_4]$ [17] which possesses a chair-like arrangement of the copper and iodine atoms: $[Cu_4(\mu_3\text{-}I)_4(PEt_3)_4]$ has a regular cubane core [18]. Selected bond lengths for each of these species are also presented in Table 1. The different structural motifs adopted by these copper iodide complexes have been associated with the relative steric demands of the phosphine ligands, with larger ligands preferring the chair conformation. In the case of $[Cu_4(\mu_3\text{-}I)_4(PPh_2Ur)_4]$, where the phosphine ligand possess a similar steric demand to PPh_3, the effect of the hydrogen-bonding network (*q.v.*) cannot be ignored.

In this solid state structure the $[Cu_4(\mu_3\text{-}I)_4(PPh_2Ur)_4]$ molecules are linked by a hydrogen bonding array which arises from interactions between uracil groups on neighbouring clusters. The uracil groups attached to the P(2) and P(3) edge of the Cu_4 tetrahedron interact *via* multiple hydrogen bonds with the groups attached to P(1) and P(4) (Fig. 3c). Considering the uracil group attached to P(4), the N–H group in the 3-position of the ring is engaged in hydrogen bonding to the carbonyl group in the 2-position of the uracil attached to P(2) [N(8)–H(8A)···O(4) 2.784(4) Å]. The oxygen atom of the carbonyl group in the 2-position of the uracil group attached to P(4) is involved in bifurcated hydrogen bonding to the N–H group in the 3-position of the uracil attached to P(2) [N(3)–H(3)···O(8) 2.744(4) Å] and N–H group in the 1-position attached to P(3) [N(6)–H(6A)···O(8) 3.007(4) Å]. On the basis of the bond lengths, however, there is considerable asymmetry in this bifurcated arrangement. The N–H group in the 3-position of the uracil attached to P(4) is engaged in hydrogen-bonding to the carbonyl group in the 2-position of the uracil attached to P(3) [N(7)–H(7A)···O(6) 2.776(4) Å]. Additionally the carbonyl group in the 2-position of the uracil attached to P(1) is engaged in hydrogen bonding with the N–H group in the 3-position of the uracil attached to P(3) [N(5)–H(5)···O(2) 2.854(4) Å]. The sum of these interactions is to create a one-dimensional hydrogen bonded strand which is propagated into a two-dimensional network by

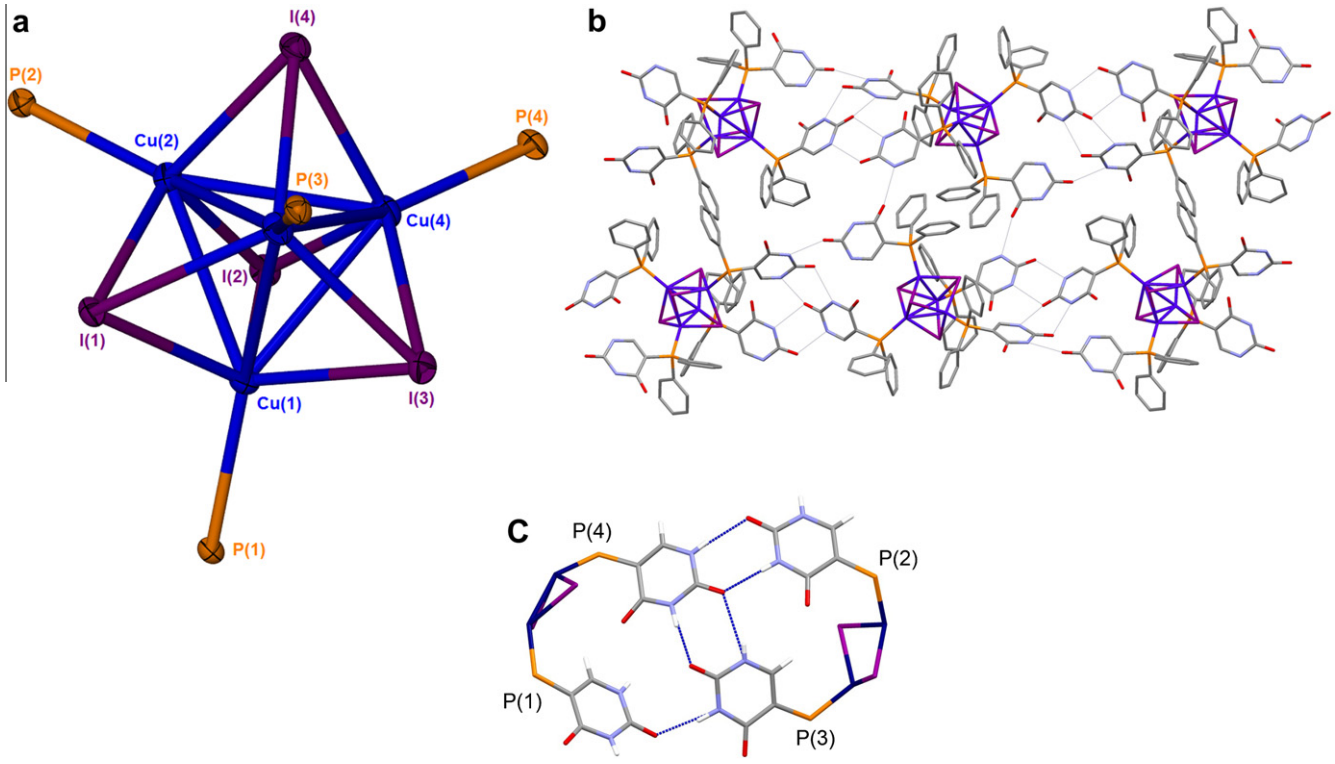

Fig. 3. (a) $[Cu(\mu_3\text{-}I)P]_4$ core of $[Cu_4(\mu_3\text{-}I)_4(PPh_2Ur)_4]$, thermal ellipsoids shown at the 50% probability level (b) hydrogen bonding network (THF molecules omitted for clarity). (c) Intermolecular hydrogen bonding motif. Copper atoms shown in dark blue, iodine in purple and phosphorus in orange. (For interpretation of the references to colours in this figure legend, the reader is referred to the web version of this article.)

Table 1
Selected bond lengths (Å) for complexes $[Cu_4(\mu_3\text{-}I)_4(PR_3)_4]$. $[Cu_4(\mu_3\text{-}I)_4(PEt_3)_4]$ has crystallographic T_d symmetry, $[Cu_4(\mu_3\text{-}I)_4(PMe_2Ph)_4]$ crystallographic C_2 symmetry and $[Cu_4(\mu_3\text{-}I)_4(PPh_3)_4]$ crystallographic C_i symmetry.

		$[Cu_4I_4(PPh_2Ur)_4]$	$[Cu_4I_4(PEt_3)_4]$ [17]	$[Cu_4I_4(PMe_2Ph)_4]$ [16]	$[Cu_4I_4(PPh_3)_4]$ [18]
Cu(1)	Cu(3)	3.0361(6)	2.9272(20)	3.0095(13)	2.8345(29)
Cu(1)	Cu(4)	2.8278(7)		2.83595(13)	4.2949(29)
Cu(2)	Cu(3)	2.9571(7)		2.9620(18)	3.4040(36)
Cu(2)	Cu(4)	2.8235(6)		2.9202(18)	
Cu(3)	Cu(4)	2.8800(6)			
Cu(1)	P(1)	2.2622(10)	2.2538(27)	2.2500(20)	2.2277(47)
Cu(2)	P(2)	2.2529(10)		2.2498(20)	2.2418(39)
Cu(3)	P(3)	2.2558(10)			
Cu(4)	P(4)	2.2560(10)			
Cu(1)	I(1)	2.6810(5)	2.6837(13)	2.7262(11)	2.5273(22)
Cu(1)	I(2)	2.6869(5)		2.6440(11)	2.5913(24)
Cu(1)	I(3)	2.6876(5)		2.7157(12)	
Cu(2)	I(1)	2.6968(5)		2.7591(11)	2.6203(23)
Cu(2)	I(2)	2.6789(5)		2.6108(11)	2.7281(23)
Cu(2)	I(4)	2.6508(5)		2.7333(12)	2.7073(22)
Cu(3)	I(1)	2.6816(5)			
Cu(3)	I(3)	2.7003(5)			
Cu(3)	I(4)	2.6453(5)			
Cu(4)	I(2)	2.6782(5)			
Cu(4)	I(3)	2.6297(6)			
Cu(4)	I(4)	2.7111(5)			
I(1)	I(2)	4.5090(4)	4.3800(11)	4.2973(12)	4.3842(17)
I(1)	I(3)	4.2774(4)		4.4883(8)	4.2044(18)
I(1)	I(4)	4.2988(4)		4.4188(9)	4.2375(22)
I(2)	I(3)	4.3906(4)		4.3253(12)	
I(2)	I(4)	4.3933(4)			
I(3)	I(4)	4.4190(4)			

hydrogen bonding between the NH in the 1-position of the uracil group attached to P(2) and the carbonyl in the 4-position on P(1) on neighbouring strands [N(4)–H(4A)···O(1) 2.857(4) Å].

It should also be noted that neither of the NH groups on the uracil groups attached to P(1) are involved in hydrogen bonding to another nucleobase. The two THF molecules that could be successfully modelled as part of the structural solution are located close in-space to these NH groups, although the nature of the disorder means that the nature of any interactions must be treated with considerable caution.

In a similar vein to $[Cu_4(\mu_3\text{-}I)_4(PPh_3)_4]$, one might expect the uracil-substituted copper complex to adopt a chair-like conformation on the basis of steric arguments. However it is tempting to argue that the effects of the hydrogen bonding network may affect the ultimate geometry of the complex. In cases such as this, where the copper core may form one several structural types with only small variations in energy, then the most favourable arrangement of the non-covalent interactions may play a role in dictating the global geometry. Therefore, although it is possible that the chair conformation may be favoured on steric grounds, the observed distorted tetrahedral shape might allow for hydrogen bonding interactions to be optimised.

2.3. Synthesis of $P(O)Ph_2Ur$

The reaction of CuI with PPh_2Ur using THF which had not been deoxygenated and dried did not form the tetrameric copper complex $[Cu_4(\mu_3\text{-}I)_4(PPh_2Ur)_4]$. In this instance colourless crystals of the phosphine oxide $P(O)Ph_2Ur$ were isolated. In addition to NMR spectroscopy and mass spectrometry, the structure of this oxide was determined by single crystal X-ray diffraction.

As shown in Fig. 4a, the asymmetric unit contained two crystallographically-independent molecules of $P(O)Ph_2Ur$ and a THF of crystallisation. The bond lengths within the two independent molecules were in general found to be statistically identical, yet two different hydrogen bonding motifs are present. In the case of the phosphine containing atom P(1), the uracil group is engaged in complementary hydrogen bonding through N(1)–H and O(2) to an identical neighbour [N(1)–H(1)···O(2) 2.836(2) Å; H(1)···O(2) 1.97(2) Å, N(1)–H(1)···O(2) 176(2)°]. The oxygen attached to P(1) exhibits a hydrogen bond to a N–H group on the other phosphine oxide molecule in the asymmetric unit, specifically to the N–H group in the 1-position of the uracil group [O(3)···H(4)–N(4) 2.738(2) Å, H(4)···O(3) 1.90(2) Å, O(3)···H(4)–N(4) 170(2)°]. The only remaining hydrogen-bonding interaction involving the uracil group attached to P(2) is between the N–H group in the 3-position and the THF of crystallisation, [N(3)–H(3)···O(7) 2.840(1) Å, H(3)···O(7) 1.90(2) Å, N(3)–H(3)···O(7) 177(2)°]. However the oxygen attached to the phosphorus atom P(2) is engaged in hydrogen bonding to the N–H group in the 1-position of the uracil group attached to P(1) [O(6)···H(1)–N(1) 2.670(1) Å, O(6)···H(1) 1.85(2), O(6)···H(1)–N(1) 177(2)°]. The net effect of these interactions is to produce a linear hydrogen bonded strand (Fig. 4b), which additionally exhibits some mutual π–π interactions between the uracil groups attached to P(2) [C(25)···N(3) 3.110(2) Å, C(26)···O(5) 3.112(2) Å] (Fig. 4c). As may be seen from the space filling diagram (Fig. 4d), the polar nucleobase and P–O units form a distinct domain surrounded by the non-polar aromatic groups. This is also the case in the structure of PPh_2Ur.

The strongest hydrogen bonds in the structure of $P(O)Ph_2Ur$ appear to be those involving the phosphine oxide functionality [19], at least on the basis of the observed bond lengths. Hydrogen bonds of the N–H···O=P type have been observed previously and that between O(6) and H–N(1) [2.6682(3) Å] is an example of an extremely short interaction of this type [20].

2.4. Synthesis of PPh_2Ur^P

A further phosphine ligand, based on the pyrimidine group, was targeted in which the hydrogen-bonding capability of the uracil group had been removed by suitable protecting groups. The synthetic procedure employed is shown in Scheme 3 and it was envisaged that such a ligand might be able to act as Brønsted base in a similar way to the more well-known pyridyl-substituted

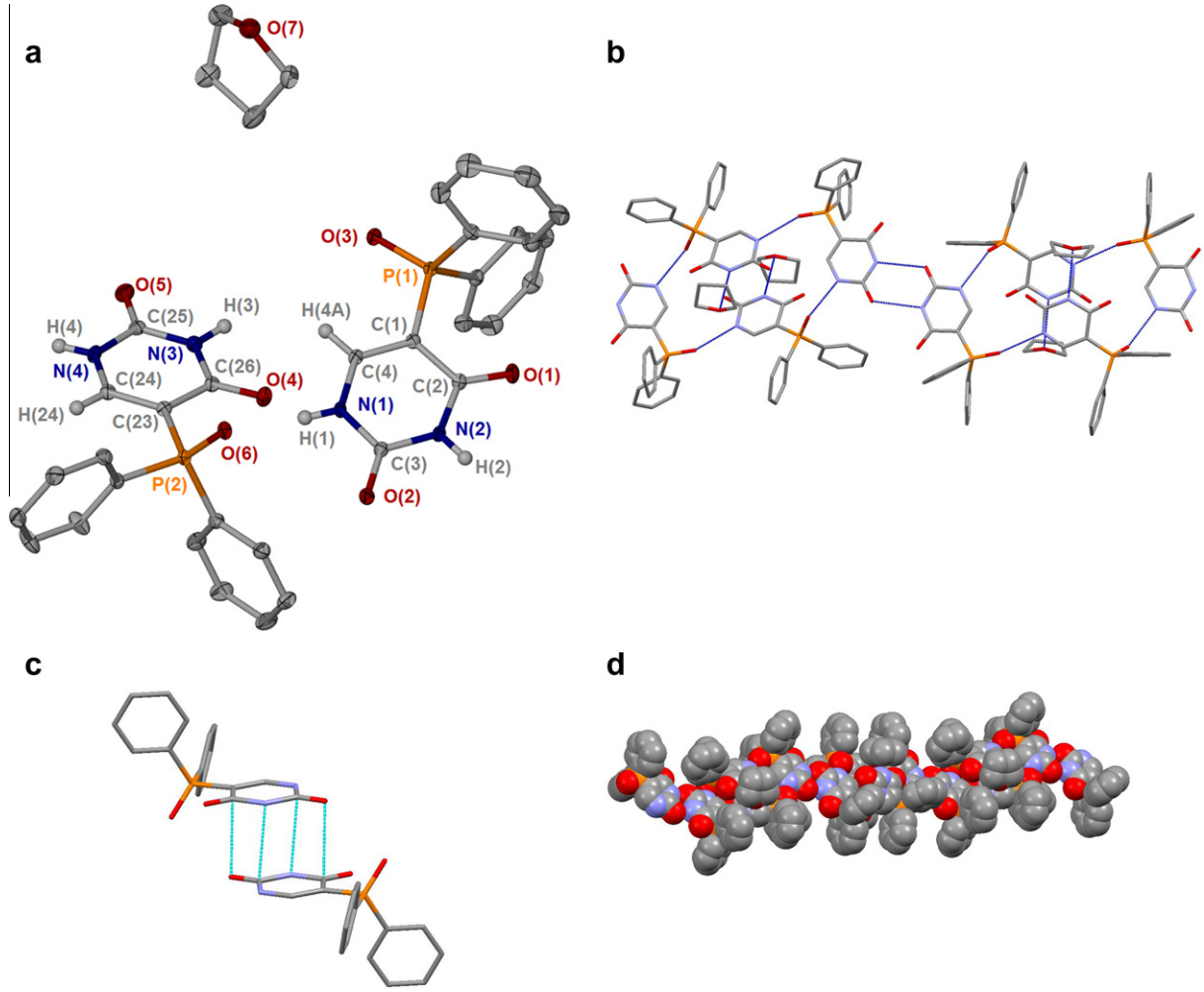

Fig. 4. (a) Asymmetric unit for $P(O)Ph_2Ur$, thermal ellipsoids shown at the 50% probability level and selected hydrogen atoms omitted for clarity. (b) Hydrogen bonded network (c) π–π interaction between uracil groups (d) space filling diagram.

phosphines. Reaction of 5-bromouracil with $POCl_3$ results in the formation of 5-bromo-2,4-dichloropyrimidine. Subsequent reaction with benzyl-alcohol and NaH results in the generation of 5-bromo-2,4-*bis*(benzyloxy)pyrimidine. The final step in the reaction procedure to prepare PPh_2Ur^P utilised the low temperature lithiation of 5-bromo-2,4-*bis*(benzyloxy)pyrimidine with Li^{n}Bu followed by addition of $PClPh_2$.

In addition to characterisation by NMR spectroscopy and mass spectrometry, the structure of PPh_2Ur^P (Fig. 5) was determined by single crystal X-ray diffraction. The resulting structure determination demonstrated that PPh_2Ur^P had crystallised in the chiral space group $P2_1$. The phosphorus atom in the PPh_2Ur^P is coordinated to two phenyl group and the benzyl-protected pyrimindine at the 5-position of the ring. Again the introduction of the pyrimidine group does not profoundly affect the structure of the phosphine when compared to PPh_3. For example, the sum of the angles at phosphorus is 305.72(14)° [C(13)–P(1)–C(1) 100.47(8)°, C(13)–P(1)–C(7) 102.02(8)°, C(1)–P(1)–C(7) 103.23(8)°] with the two angles involving the pyrimidine group slightly more acute that the remaining one between the two phenyls. Furthermore, the P–C bonds to the two phenyl groups are similar [C(7)–P(1) 1.8321(19) Å, C(1)–P(1) 1.830(2) Å] whereas that to the pyrimidine is somewhat shorter [C(13)–P(1) 1.8216(18) Å].

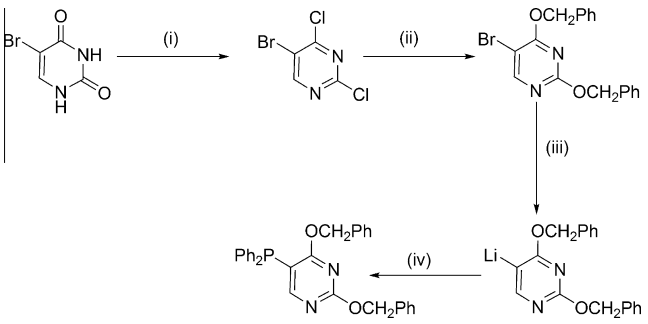

Scheme 3. (i) $+POCl_3$; (ii) +NaH, $+HOCH_2Ph$; (iii) $+Li^nBu$ (−85°); (iv) $+PClPh_2$.

2.5. Synthesis of $[Ru(\eta^5\text{-}C_5H_5)(NCMe)(PPh_2Ur^P)_2]PF_6$

The half-sandwich complex $[Ru(\eta^5\text{-}C_5H_5)(NCMe)(PPh_2Ur^P)_2]PF_6$ was prepared in order to investigate the potential of PPh_2Ur^P to direct the ruthenium-mediated hydration of alkynes. The reaction of $[Ru(\eta^5\text{-}C_5H_5)(NCMe)_3]PF_6$ with two equivalents of PPh_2Ur^P was initially investigated by NMR spectroscopy in $CDCl_3$ solution. The resulting $^{31}P\{^1H\}$ NMR spectrum exhibited a new singlet resonance at δ 30.7 corresponding to the formation of the cation $[Ru(\eta^5\text{-}C_5H_5)(NCMe)(PPh_2Ur^P)_2]^+$. Slow diffusion of Et_2O into this solution resulted in the formation of yellow crystals of the complex suitable

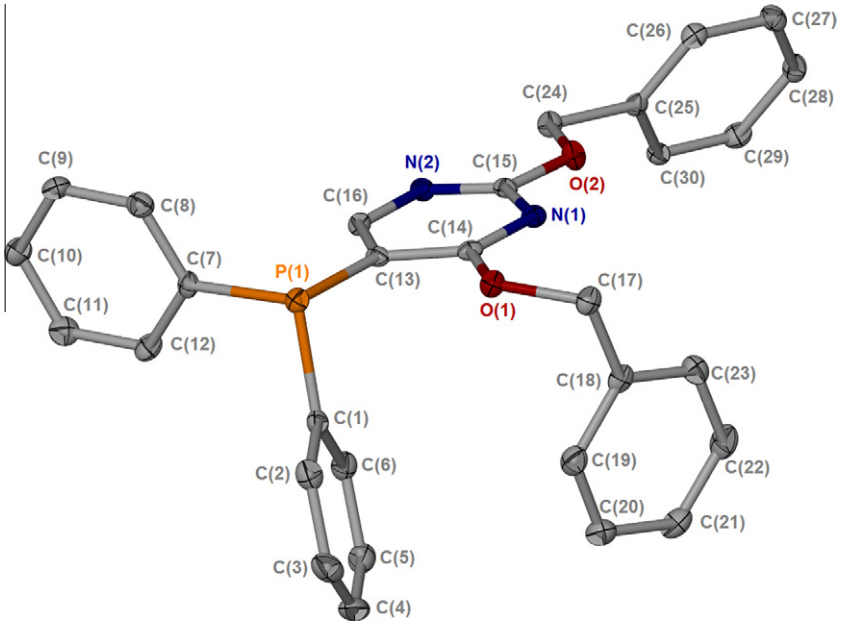

Fig. 5. Structure of PPh_2Ur^P in the solid state. Thermal ellipsoids are shown at the 50% probability level, hydrogen atoms omitted for clarity.

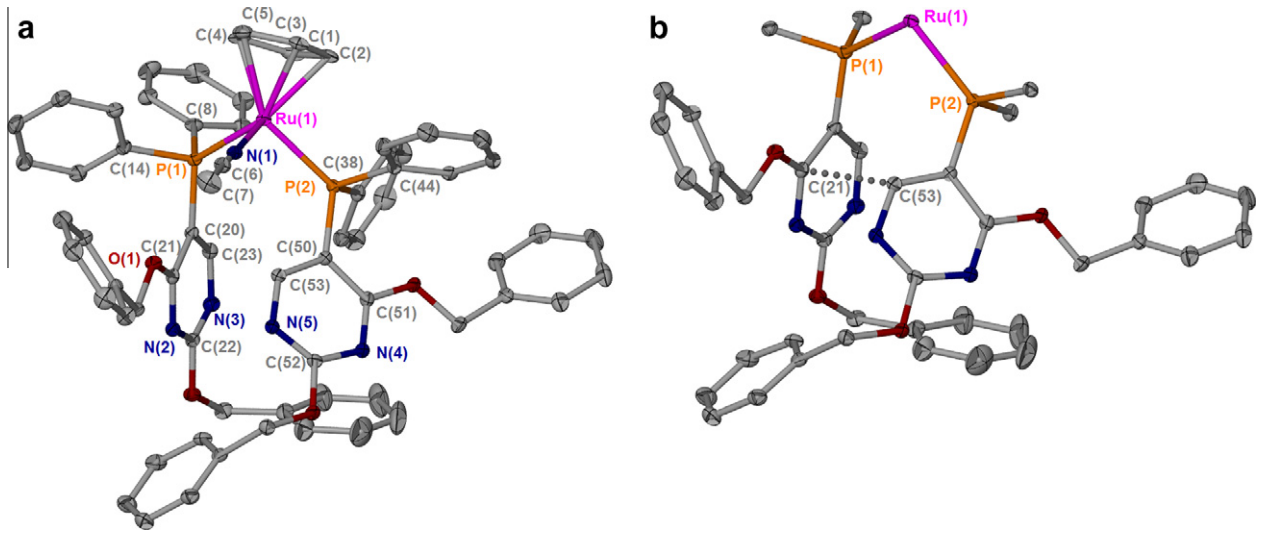

Fig. 6. (a) Structure of the cation $[Ru(\eta^5\text{-}C_5H_5)(NCMe)(PPh_2Ur^P)_2]^+$. Thermal ellipsoids shown at the 50% probability level and hydrogen atoms omitted for clarity. (b) Coordination environments of the PPh_2Ur^P ligands.

for study by X-ray diffraction. The resulting study demonstrated that the complex had crystallised as a mixed $Et_2O/CDCl_3$ solvate in the triclinic space group $P\bar{1}$: the structure of the cation is shown in Fig. 6a.

The structure determination demonstrated that the complex did indeed contain two PPh_2Ur^P ligands with the remaining coordination sites being occupied by cyclopentadienyl and acetonitrile ligands. The phosphine ligands are both arranged so that the two phenyl groups are directed towards the cyclopentadienyl ligand, thus the benzyl-protected pyrimidine groups provide a sterically-hindered region around the remaining faces of the complex, Fig. 6(b). There is a close contact between the pyrimidine rings [C(21)–C(53) 3.247(3) Å] which may be indicative of a π–π interaction. This may, at least in the solid-state, assist in defining the topology of the coordination sphere of the metal.

The potential for $[Ru(\eta^5\text{-}C_5H_5)(NCMe)(PPh_2Ur^P)_2]PF_6$ to act as a catalyst for the hydration of phenyl acetylene was investigated. Unfortunately, only a slow reaction occurred and the major product proved to be the linear dimer of the alkyne, *E*-1,4-diphenyl-1-buten-3-yne [21]: only trace amount of hydration products were observed.

3. Conclusions

The solid-state structure of the phosphine PPh_2Ur and its oxide $P(O)Ph_2Ur$ show a number of common features, most notably the clustering of polar and non-polar domains. In some respects the topology may be compared to that of double strand nucleic acids with the bases contained with a sheath of (in this instance) a very non-polar aromatic region or (in the case of nucleic acids) a water-solubilising phosphate backbone. Clearly, by removing the N–H and carbonyl functionality by protection with benzyl-groups the potential for the pyrimidine to engage in hydrogen bonding is all

but removed as demonstrated by the structures of PPh_2Ur^P and its ruthenium complex.

In a similar vein to Kamer and co-workers [11], we have also shown that it is possible to use palladium-mediated methods to prepare uracil functionalised phosphine ligands and, in addition, that a salt-elimination method may be used to prepare pyrimidine-substituted phosphine PPh_2Ur^P. Therefore, the preparation of related functionalised phosphorus(III) ligands should be possible by extension of these synthetic methods and thus expand the library of ligands that may engage in hydrogen bonding for both catalytic and structural purposes.

4. Experimental

Unless otherwise stated, all reactions were performed under an atmosphere of dry nitrogen using standard Schlenk line and glove box techniques. THF was distilled from sodium/benzophenone, NEt_3 was distilled from sodium and degassed before use, Et_2O was purified using an Innovative Technology anhydrous solvent engineering system. $CDCl_3$ was dried over CaH_2 and vacuum transferred prior to use. 5-iodouracil, $[Ru(\eta^5\text{-}C_5H_5)(NCMe)_3][PF_6]$ and DMF (anhydrous) were purchased from Aldrich. 5-Bromo-2,4-dichloropyrimidine [22] and 5-bromo-2,4-bis(benzyloxy)pyrimidine [23] were prepared according to literature procedures.

NMR spectra were recorded on either a Bruker AV500 (operating frequencies ^1H 500.13 MHz, ^{31}P 202.50 MHz, ^{13}C 125.77 MHz), or JEOL EX400 (operating frequencies ^1H 400.13 MHz, ^{31}P 161.83 MHz, ^{13}C 100.60 MHz) spectrometers. $N = {}^nJ_{PC} + {}^{(n+2)}J_{PC}$. Mass spectra were acquired using the ESI technique on a Bruker Daltronic microTOF instrument.

4.1. Synthesis of PPh_2Ur

A Schlenk tube containing a magnetic stirrer bar was charged with 5-iodouracil (0.34 g, 1.41 mmol), DMF (10 ml), NEt_3 (0.22 ml, 1.55 mmol) and PPh_2H (0.26 ml, 1.55 mmol). $Pd(OAc)_2$ (3 mol%, 9.5 mg) was added and the resulting deep purple solution heated at 60 °C for 1 h. The solvent was removed under reduced pressure and the residue purified by dissolution warm methanol, any insoluble impurities were removed by filtration. Cooling the solution to −20 °C resulted in the formation of a precipitate of PPh_2Ur which could be further recrystallized until the sample was colourless. Yield 159 mg (38%).

^1H NMR (d_6-DMSO) δ 11.28 (s, 1H, N***H***), δ 10.96 (s, 1H, N***H***), δ 7.42–7.25 (10H, ***Ph***), δ 6.45 (1H, Ur C***H***). $^{31}P\{^1H\}$ NMR (d_6-DMSO) δ −21.1 (s). $^{13}C\{^1H\}$ δ 164.2 (d, J_{PC} = 18.8 Hz, ***C***=O), δ 151.2 (s, ***C***=O), 144.5 (d, J_{PC} = 9.9 Hz, ***C***H) δ 135.2 (d, J_{PC} = 10.8 Hz, ***Ph***), δ 133.2 (d, J_{PC} = 20.4 Hz, ***Ph***), 129.1 (s, ***Ph***) 128.7 (d, J_{PC} = 6.8 Hz, ***Ph***), 107.4 (s, Ur ***C***^{5}). Mass spectrum 297.0788 ($M+H^+$ expected for $C_{16}H_{14}N_2O_2P$ 297.0787), 319.0605 ($M+Na^+$ expected for $C_{16}H_{13}N_2NaO_2P$ 319.0607). IR (ATR/cm^{-1}) 3285 (br, m) 3126 (br, w) 3031 (br, w), 2827 (w), 1779 (w), 1739 (m) 1699 (m), 1646 (s), 1607 (s), 1466 (m), 1423 (m), 1324 (m) 1215 (m), 1137 (s), 1048 (w) 939 (w) 886 (w) 850 (w), 776 (w) 756 (m), 732 (m) 635 (m). Elemental *Anal.* Calc. for $C_{16}H_{13}N_2O_2P$: C, 64.87; H, 4.42; N, 9.46. Found: C, 64.57; H, 4.45; N, 9.35%.

4.2. Synthesis of $[Cu_4(\mu_3\text{-}I)_4(PPh_2Ur)_4]$

Copper iodide (13 mg, 0.09 mmol) and PPh_2Ur (20 mg, 0.08 mmol) were added to dry THF (2 ml) and the mixture shaken. Any insoluble residues were removed by filtration and hexane (2 ml) was allowed to diffuse into the resulting solution resulting in the formation of colourless crystals of $[Cu_4(\mu_3\text{-}I)_4(PPh_2Ur)_4]$.

4.3. Synthesis of $P(O)Ph_2Ur$

$P(O)PPh_2Ur$ was prepared using an identical procedure to $[Cu_4(\mu_3\text{-}I)_4(PPh_2Ur)_4]$ with the exception that the THF employed was not purified prior to use. Yield 9 mg (38%) ^1H NMR (d_6-DMSO) δ 10.78 (br. s, 1H, N***H***), 10.51 (s, 1H, N***H***), 6.80 (d, J_{HP} = 10.9 Hz, 1H, CH), 6.85 (ddd, $^3J_{HP}$ = 12.8 Hz, $^3J_{HH}$ = 7.5, $^4J_{HH}$ = 1.0 Hz, 4H, ***Ph***), 6.70 (dd, $^3J_{HH}$ = 7.5 Hz, $^4J_{HH}$ = 1.0 Hz, 2H, ***Ph***), 6.62 (td, $^3J_{HH}$ = 7.5 Hz, $^4J_{HP}$ = 2.8 Hz, 4H, ***Ph***). $^{31}P\{^1H\}$ NMR (d_6-DMSO) δ 22.3 (s). $^{13}C\{^1H\}$ δ 162.7 (d, J_{PC} = 10.5 Hz, ***C***=O), 151.2 (s, ***C***=O), 150.9 (d, J_{PC} = 12.8 Hz, C***H***), 132.5 (d, J_{PC} = 110 Hz, ***Ph***), 131.9 (d, J_{PC} = 3.0 Hz, ***Ph***), 131.4 (d, J_{PC} = 10.5 Hz, ***Ph***), 128.4 (d, J_{PC} = 12.5 Hz, ***Ph***), 103.1 (br, Ur ***C***^{5}). Mass spectrum 313.0736 ($M+H^+$ expected for $C_{16}H_{14}N_2O_3P$ 313.0737), 335.0552 ($M+Na^+$ expected for $C_{16}H_{13}N_2NaO_3P$ 335.0556) IR (ATR/cm^{-1}) 3469 (br, w), 3271 (br, w), 2962 (br, w), 1768 (m) 1714 (m) 1611 (w), 1483 (w), 1407 (m), 1165 (m), 1036 (m), 990 (w), 694 (w). Elemental *Anal.* Calc. for $C_{16}H_{13}N_2O_3P\cdot(THF)_{0.5}$: C, 62.07; H, 4.92; N, 8.04. Found: C, 62.18; H, 5.24; N, 7.88%.

4.4. Synthesis of PPh_2Ur^P

A dry 100 ml flask, equipped with a septum, inlet, low temperature thermometer, and magnetic stirrer bar was flushed with argon. A solution of 5-bromo-2,4-*bis*(benzyloxy)pyrimidine (0.5 g, 1.3 mmol) in THF (35 ml) was introduced and the flask and cooled to −95 °C. A pre-cooled solution of *n*-BuLi (2.5 M solution in hexanes, 1.6 mmol) was added at such a rate that the internal temperature did not exceed −85 °C. The yellow solution was stirred for 5 min then chlorodiphenylphosphine (313 µl, 1.7 mmol) was added and temperature maintained for a further 20 min then allowed to warm to room temperature over 2 h. The solution was evaporated to dryness and the residue extracted with methanol. The resulting solution was concentrated *in vacuo*, cooling to −20 °C resulted in the formation of colourless crystals. Yield = 247 mg (40%).

^1H NMR ($CDCl_3$) δ 7.67 (d, $^3J_{HP}$ = 2.8 Hz, 1H, C***H***), 7.46 (m, 2H, ***Ph***), 7.35 (m, 13H, ***Ph***), 7.20 (m, 3H, ***Ph***), 6.98 (m, 2H, ***Ph***), 5.39 (s, 2H, C***H***$_2$), 5.37 (s, 2H, C***H***$_2$). $^{31}P\{^1H\}$ NMR ($CDCl_3$) -23.5 (s). $^{13}C\{^1H\}$ NMR ($CDCl_3$) 171.2 (d, $^2J_{PC}$ = 14.6 Hz, ***C***OCH$_2$), 165.7 (s, ***C***OCH$_2$), 162.6 (d, $^2J_{PC}$ = 7.0 Hz, ***C***H), 136.5 (s, CH$_2$***Ph***, C^1) 135.9 (s, CH$_2$***Ph***, C^1), 134.7 (d, $^1J_{CP}$ = 9.8 Hz, P***Ph***, C^1), 134.0 (s, ***Ph***), 133.8 (s, ***Ph***), 129.3 (s, ***Ph***), 128.8 (d, $^3J_{PC}$ = 7.4 Hz, P***Ph***, C^3), 128.6 (s, ***Ph***), 128.3 (d, $^2J_{PC}$ = 8.8 Hz, P***Ph***, C^2), 128.2 (s, CH$_2$***Ph***, C^4), 127.8 (s, CH$_2$***Ph***, C^4), 127.4 (s, ***Ph***), 110.8 (d, $^1J_{PC}$ = 17.8 Hz, Ur^P ***C***^{5}), 69.4 (s, ***CH***$_2$Ph), 68.4 (s, ***CH***$_2$Ph). Mass spectrum 477.1727 ($M+H^+$ expected for $C_{30}H_{26}N_2O_2P$ 477.1726). IR (ATR/cm^{-1}) 3066 (w), 1566 (m), 1444 (m) 1454 (m), 1410 (m), 1353 (m), 1267 (m), 1227 (m), 1098 (m), 1041 (m), 979 (m), 905 (w), 852 (w), 796 (m), 745 (m), 697 (s). Elemental *Anal.* Calc. for $C_{30}H_{25}N_2O_2P$: C, 75.62; H, 5.29; N, 5.88. Found: C, 73.89; H, 4.93; N, 5.74%. Repeats of the analysis gave similar results with good matches to predicted hydrogen and nitrogen content, but less carbon than expected.

4.5. Synthesis of $[Ru(\eta^5\text{-}C_5H_5)(NCMe)(PPh_2Ur^P)_2][PF_6]$

$[Ru(\eta^5\text{-}C_5H_5)(NCMe)_3][PF_6]$ (30 mg, 6.91×10^{-5} mol) and PPh_2Ur^P (66 mg, 1.39×10^{-4} moles) were dissolved in $CDCl_3$ in an NMR tube fitted with a PTFE ampoule. A $^{31}P\{^1H\}$ NMR spectrum was then recorded to ensure that the reaction had reached completion. The solution was transferred into an ampoule and Et_2O allowed to slowly diffuse into the solution to precipitate the product which could subsequently isolated by filtration.

^1H NMR ($CDCl_3$): δ = 8.01 (s, 2H, C***H***), 7.5–6.5 (20 H, ***Ph***) 5.40 (m, 4H, C***H***$_2$Ph), 5.12 (m, 4H, C***H***$_2$Ph), 4.23 (s, 5H, C$_5$***H***$_5$), 1.62 (s, 3H, NCC***H***$_3$), $^{31}P\{^1H\}$ NMR ($CDCl_3$): δ = 30.7 (s, ***P***Ph$_3$), −133.3 (septet,

Table 2
Data collection and structural refinements details for single crystal X-ray diffraction studies of compounds reported.

	$PPh_2Ur{\cdot}MeOH$	$[Cu_4(\mu^3\text{-}I)_4(PPh_2Ur)_4]{\cdot}2THF$	$P(O)Ph_2Ur{\cdot}0.5THF$	PPh_2Ur^P	$[Ru(\eta^5\text{-}C_5H_5)(NCMe)(PPh_2Ur^P)_2][PF_6](CHCl_3)_{0.75}(Et_2O)_{0.25}$
Empirical formula	$C_{17}H_{17}N_2O_3P$	$C_{72}H_{59}Cu_4I_4N_8O_{10}P_4$	$C_{18}H_{17}N_2O_{3.5}P$	$C_{30}H_{25}N_2O_2P$	$C_{68.75}H_{61.25}Cl_{2.25}F_6N_5O_{4.25}P_3Ru$
Formula weight	328.30	2081.91	348.31	476.49	1413.22
T (K)	100(2)	110	110.0	100(2)	110(2)
λ (Å)	0.71073				
Crystal system	monoclinic	monoclinic	monoclinic	monoclinic	triclinic
Space group	$P2(1)/c$	$P2(1)/n$	$C2/c$	$P2(1)$	$P\bar{1}$
a (Å)	17.7803(15)	12.9440(9)	17.1552(17)	11.6311(13)	13.3175(9)
b (Å)	5.4182(5)	24.1550(16)	14.8765(15)	5.5875(6)	14.6515(10)
c (Å)	18.4514(15)	30.384(2)	26.674(3)	18.225(2)	18.0383(12)
α (°)	90	90	90	90	108.6640(10)°
β (°)	114.416(2)	98.680(2)	102.987(2)	95.554(2)°.	93.0410(10)
γ (°)	90	90	90	90	102.6260(10)
V (Å^3)	1618.6(2)	9391.3(11)	6633.3(12)	1178.9(2)	3225.0(4)
Z	4	4	16	2	2
D_{calc} (mg m^{-3})	1.347	1.472	1.395	1.342	1.455
Absorption coefficient (mm^{-1})	0.186	2.327	0.188	0.148	0.482
$F(000)$	688	4060	2912	500	1448
Crystal size (mm^3)	0.28 × 0.12 × 0.06	0.23 × 0.11 × 0.02	0.45 × 0.10 × 0.05	0.38 × 0.12 × 0.04	0.14 × 0.06 × 0.05
ϕ Range for data collection (°)	2.22–28.33	1.60–28.31	1.57–28.31	1.76–28.32	1.20–30.03
Index ranges	$-23 \leqslant h \leqslant 23$	$-17 \leqslant h \leqslant 17$	$-22 \leqslant h \leqslant 22$	$-15 \leqslant h \leqslant 15$	$-18 \leqslant h \leqslant 18$
	$-7 \leqslant k \leqslant 7$	$0 \leqslant k \leqslant 32$	$-19 \leqslant k \leqslant 19$	$-7 \leqslant k \leqslant 7$	$-20 \leqslant k \leqslant 20$
	$-24 \leqslant l \leqslant 24$	$0 \leqslant l \leqslant 40$	$-35 \leqslant l \leqslant 35$	$-24 \leqslant l \leqslant 24$	$-25 \leqslant l \leqslant 24$
Reflections collected	15105	23288	33496	12088	36912
Independent reflections (R_{int})	4020 (0.0327)	23288 (0.0542)	8225 (0.0238)	5843 (0.0292)	18195 (0.0275)
Completeness to theta	99.6 (to 28.33)	99.6 (to 28.31)	99.7 (to 28.31)	99.7 (to 28.32)	96.4 (to 30.03)
Absorption correction	Semi-empirical from equivalents				
Max. and min. transmission	0.990 and 0.813	1.000 and 0.842	1.000 and 0.864	0.990 and 0.847	0.976 and 0.820
Refinement method	Full-matrix least-squares on F^2				
Data/restraints/parameters	4020/0/221	23288/18/965	8225/0/458	5843/1/316	18195/0/851
Goodness-of-fit (GOF) on F^2	1.038	0.921	1.016	1.004	1.031
Final R indices [$I > 2\sigma(I)$]	$R_1 = 0.0387$	$R_1 = 0.0364$	$R_1 = 0.0372$	$R_1 = 0.0414$	$R_1 = 0.0372$
	$wR_2 = 0.1000$	$wR_2 = 0.0763$	$wR_2 = 0.0944$	$wR_2 = 0.0847$	$wR_2 = 0.0877$
R indices (all data)	$R_1 = 0.0555$	$R_1 = 0.0667$	$R_1 = 0.0443$	$R_1 = 0.0484$	$R_1 = 0.0571$
	$wR_2 = 0.1099$	$wR_2 = 0.0829$	$wR_2 = 0.0984$	$wR_2 = 0.0877$	$wR_2 = 0.0977$
Largest diff. peak and hole (eÅ^{-3})	0.434/−0.279	1.108/−0.684	0.501/−0.281	0.311/−0.215	0.706/−0.895
Absolute structure parameter (Flack)				−0.03(8)	

$^1J_{PF}$ = 712.8 Hz, $\mathbf{P}F_6$), $^{13}C\{^1H\}$ NMR ($CDCl_3$): δ = 169.8 (s, $\mathbf{C}OCH_2$), 166.4 (s, $\mathbf{C}OCH_2$), 164.9 (t, N = 17 Hz, $\mathbf{C}H$), 136.1 (s, C^1, ***Ph***), 134.6 (s C^1, ***Ph***) 133.1 (t, N = 10.2 Hz, ***Ph***), 131.8 (t, N = 10.2 Hz, ***Ph***), 131.5 (partially obscured C^1, ***Ph***), 130.5 (s, ***Ph***, C^4), 128.7 (s, ***Ph***, C^4), 128.6 (m, ***Ph***), 128.5 (m, ***Ph***), 128.3 (s, ***Ph***), 128.2 (s, ***Ph***), 107.5 (t, N = 34.7 Hz, Ur^P $\mathbf{C}_5$) 84.3 ($\mathbf{C}_5H_5$), 69.9 ($\mathbf{C}H_2$), 69.7 ($\mathbf{C}H_2$), 66.0 ($N\mathbf{C}CH_3$), 3.33 ($NC\mathbf{C}H_3$). Elemental *Anal.* Calc. for $[Ru(\eta^5\text{-}C_5H_5)(NCMe)(PPh_2Ur^P)_2][PF_6](CHCl_3)_{0.75}(Et_2O)_{0.25}$: C, 59.01; H, 4.41; N, 4.00. Found: C, 58.58; H, 4.45; N, 3.84%.

4.6. Details of X-ray diffraction experiments

Details of the collection and refinement are presented in Table 2. Diffraction data were collected at 110 K on a Bruker Smart Apex diffractometer with Mo Kα radiation (λ = 0.71073 Å) using a SMART CCD camera. Diffractometer control, data collection and initial unit cell determination was performed using "SMART" [24]. Frame integration and unit-cell refinement software was carried out with "SAINT+" [25]. Absorption corrections were applied by SADABS (v2.03, Sheldrick). Structures were solved by direct methods using SHELXS-97 and refined by full-matrix least squares using SHELXL-97 [26]. All non-hydrogen atoms were refined anisotropically. Full details of the refinements for each structure are provided as Supplementary information in the CIF format.

Acknowledgements

We are grateful to the EPSRC (Grant *EP/R02178*) for funding of this work and Dr. N.J. Wood for informative discussions.

Appendix A. Supplementary material

Supplementary data associated with this article can be found, in the online version, at doi:10.1016/j.ica.2011.10.058.

References

[1] G.W. Parshall, S.D. Ittel, Homogeneous Catalysis : The Applications and Chemistry of Catalysis by Soluble Transition Metal Complexes, Wiley, New York, 1992. ISBN: 978-0471538295;
P.W.N.M. van Leeuwen, P.C.J. Kamer, J.N.H. Reek, P. Dierkes, Chem. Rev. 100 (2000) 2741;
W. Tang, X. Zhang, Chem. Rev. 103 (2003) 3029;
N. Fey, A.G. Orpen, J.N. Harvey, Coord. Chem. Rev. 253 (2009) 704.
[2] C.A. Tolman, Chem. Rev. 77 (1977) 313.
[3] See for example: D.G. Gusev, Organometallics 28 (2009) 763 (and references therein).
[4] D.B. Grotjahn, Dalton Trans. (2008) 6497.
[5] B. Breit, W. Seiche, Angew. Chem., Int. Ed. 44 (2005) 1640;
T. Smeikal, B. Breit, Angew. Chem., Int. Ed. 47 (2008) 311.
[6] F. Chevallier, B. Breit, Angew. Chem., Int. Ed. 45 (2006) 1599.
[7] J.M. Lynam, Dalton Trans. (2008) 4067.
[8] M.J. Cowley, J.M. Lynam, A.C. Whitwood, Dalton Trans. (2007) 4427.
[9] H. Hamidov, J.C. Jeffery, J.M. Lynam, Chem. Commun. (2004) 1364;
M.J. Cowley, J.M. Lynam, R.S. Moneypenny, A.C. Whitwood, A.J. Wilson, Dalton Trans. (2009) 9529.
[10] M.J. Cowley, J.M. Lynam, A.C. Whitwood, J. Organometal. Chem. 695 (2010) 18.
[11] L. Ropartz, N.J. Meeuwenoord, G.A. van der Marel, P.W.N.M. van Leeuwen, A.M.Z. Slawin, Paul C.J. Kamer, Chem. Commun. (2007) 1556.
[12] T.D. Nixon, L.D. Dingwall, J.M. Lynam, A.C. Whitwood, Chem. Commun. (2009) 2890.
[13] B.J. Dunne, A.G. Orpen, Acta Crystallogr., Sect. C 47 (1991) 345.
[14] A.N. Chekhlov, Kristallografiya (Russ.) (Crystallogr. Rep.) 38 (1993) 79.
[15] J. Bruckmann, C. Krüger, F. Lutz, Z. Naturforsch., B 50 (1995) 351.
[16] M.R. Churchill, F.J. Rotella, Inorg. Chem. 16 (1977) 3267.
[17] M.R. Churchill, B.G. DeBoer, D.J. Donovan, Inorg. Chem. 14 (1975) 617.

[18] M.R. Churchill, K.L. Kalra, Inorg. Chem. 13 (1974) 1899.
[19] J.L. Cook, C.A. Hunter, C.M.R. Low, A. Perez-Velasco, J.G. Vinter, Angew. Chem. Int. Ed. 46 (2007) 3706.
[20] M.C. Etter, P.W. Baures, J. Am. Chem. Soc. 110 (1988) 639;
M.C. Etter, R.D. Gillard, W.B. Gleason, J.K. Rasmussen, R.W. Duerst, R.B. Johnson, J. Org. Chem. 51 (1986) 5405;
M. Akazome, S. Suzuki, Y. Shimizu, K. Henmi, K. Ogura, J. Org. Chem. 65 (2000) 6917;
P.C. Kunz, W. Huber, B. Spingler, J. Chem. Crystallogr. 41 (2011) 105.
[21] J.M. Lynam, T.D. Nixon, A.C. Whitwood, J. Organometal. Chem. 693 (2008) 3103.
[22] G.E. Hilbert, E.F. Jansen, J. Am. Chem. Soc. 56 (1934) 134.
[23] R.F. Schinazi, W.H. Prusoff, J. Org. Chem. 50 (1985) 841.
[24] Smart diffractometer control software (v5.625), Bruker-AXS, Bruker AXS GmbH, Karlsruhe, Germany.
[25] Saint+ (v6.22) Bruker AXS, Bruker AXS GmbH, Karlsruhe, Germany.
[26] G.M. Sheldrick, Acta Crystallogr., Sect. B 64 (2008) 112.